Molecular Simulation of Poly-α-olefin Synthetic Lubricants: Impact of Molecular Architecture on Performance Properties

Loukas I. Kioupis and Edward J. Maginn

Department of Chemical Engineering, University of Notre Dame, Notre Dame, Indiana 46556

Received: July 14, 1999; In Final Form: September 21, 1999

Equilibrium and nonequilibrium molecular dynamics simulations are performed at constant pressure and temperature on three structurally distinct poly-α-olefin (PAO) isomers representative of a major component in synthetic motor oil basestock. In agreement with empirical observations, the temperature dependence of viscosity, as characterized by the viscosity number (VN), is reduced as the degree of branching is lowered. A molecular-level explanation for this behavior is given in terms of the energy barriers for intramolecular reorientation. Other dynamic properties, such as the diffusivity and rate of tumbling, were also computed and found to have similar dependencies on temperature as the viscosity. Based on these calculations, it appears that PAO molecules with long, widely spaced branches should yield a higher VN than those with short, closely spaced branches. The impact of shear rate on PAO properties is also investigated. High shear rates and shear-thinning increases the VN because the behavior of the fluid is largely dominated by the flow field rather than by the thermodynamic state point. Contrary to what has been observed with linear alkanes, it is observed that molecular alignment with the flow field does not always correlate with enhanced shear-thinning. These observations are explained in terms of a competition between the shear forces responsible for aligning the molecules and intermolecular forces that resist shear-thinning. The results of the present work provide molecular-level explanations for the favorable lubricant properties exhibited by "star-like" molecules and suggest an important strategy for assisting in a more rational approach toward the development of improved lubricants and additives.

1. Introduction

Poly-α-olefines (PAOs) are low molecular weight branched saturated hydrocarbons obtained from the catalytic oligomerization of middle-ranged (C_6–C_{20}) linear α-olefines (1-alkenes). PAOs have been found to have lubrication properties superior to that of naturally occurring "mineral oil" and are thus a major component in high-grade synthetic motor oil basestock. Some of the favorable properties of high-performance synthetic oils include excellent friction and wear characteristics, good oxidative and thermal stability, a wide operating temperature range, low volatility, compatibility with typical lubricant additives, small viscosity loss due to shearing, and biodegradability. PAOs are particularly attractive because of their low production cost, the fact that they also exhibit low "pour points" (i.e., low crystallization temperatures), and because they resist large reductions in viscosity with increasing temperature. This latter property is particularly important for engine oils. It is desirable to have the lubricant flow easily upon "cold starting" an engine, but at high operating temperatures the oil should have a high enough viscosity to maintain a fluid film between moving parts to prevent metal contact and wear.

The temperature dependence of the viscosity of a lubricant is typically characterized by the viscosity index (VI).[1] The VI is determined using a standard method (ASTM D-2270) in which the kinematic viscosity of an oil at 40 and 100 °C is compared against the viscosities of two reference oils. Alternatively, an empirical analytic expression[2] can be used. For lubricants with similar kinematic viscosities, the one with the

higher VI is "better" in the sense that it exhibits smaller changes in viscosity with temperature. The viscosity index has its origins in the early days of the petroleum industry[3] and is widely used to compare lubricants, despite the fact that there are several problems with it as a quantitative measure of lubricant performance.[2,4] One of the major problems with the VI is that it is undefined for lubricants with a kinematic viscosity <2 cSt at 100 °C.

Recently, the "viscosity number" (VN) has been proposed as an alternative measure of the temperature dependence of lubricant viscosities.[4] The VN is applicable to a wider range of lubricants than is the VI. It is also valid over a broader range of temperatures and is easy to compute. The VN has been shown to correlate well with the VI in most cases. For these reasons, the VN has been adopted in the work described here.

To compute the VN of a fluid, the kinematic viscosity is measured at 40 and 100 °C (as is the case for the determination of the VI). These values are then substituted into the Walther equation

$$\log \log(\nu + 0.7) = A + B \log T \qquad (1)$$

where ν is the kinematic viscosity in centistokes (cSt), and T the temperature in degrees Kelvin. The Walther equation has been shown to accurately capture viscosity versus temperature data for typical mineral oil and synthetic lubricants. It also forms the basis for the American Society for Testing and Materials (ASTM) viscosity–temperature chart (ASTM D341), which is quite successful in correlating the viscosity–temperature dependence of lubricants and other petroleum products. The coefficient B is determined from eq 1 and is substituted into

* Corresponding author. Telephone: (219) 631-5687. Fax: (219) 631-8366. E-mail: ed@nd.edu. Website: http://www.nd.edu/~ed.

the following expression for the VN

$$VN = \left(1 + \frac{3.55 + B}{3.55}\right) \times 100 \qquad (2)$$

As is the case for the VI, the larger the VN, the smaller the change in viscosity with temperature. The value of 3.55 has been chosen because it has been observed that lubricating oils with VI = 100 have values of B close to −3.55. Thus, it was arbitrarily established that VN = 100 when $B = -3.55$. For $B = 0$, the VN equals its maximum value of 200, which corresponds to a "perfect" oil in which the viscosity is independent of temperature.

Another alternative to the VI is to assume the viscosity is captured by an Eyring model of the form

$$\nu = A \exp(E/T) \qquad (3)$$

where E is an activation energy. Large activation energies correspond to large changes in viscosity with temperature (and hence small VI or VN).

Most PAOs in use consist of a mixture of dimer through pentamer oligomers of the starting 1-alkene material[5,6] Theoretically, the number of isomers that can be formed during the oligomerization process is staggering. For example, it has been estimated that oligomers of 1-decene in the C_{30} and C_{40} range can have well over 6×10^{13} isomer structures.[7] This large number of structures presents the lubricant formulator with two major problems: (1) Which of the countless PAO isomers produce a lubricant with superior performance properties? (2) Given a target isomer, how does one go about tailoring the reaction conditions such that the desired species is formed at high levels? Recent advances in synthetic techniques are beginning to answer the second question[5,6,8] but the answer to the first question is still very much open for debate. This answer is the focus of the present work; that is, we wish to address the way in which the molecular architecture of a given PAO isomer relates to its lubricant performance properties, such as the VI. The goal is not only to develop qualitative structure−property relations but to also provide quantitative, molecular-level explanations for the observed behavior. Ultimately, such information could be useful in helping focus synthesis efforts on compounds that have a high likelihood of having desirable properties.

There has been a great deal of experimental research conducted to determine structure−property relations for PAOs.[5,9] The most important factors that determine the properties of PAO basestocks are molecular weight and skeletal structure. One characteristic that has been found empirically to correlate well with lubricant properties is the so-called "branch ratio", which is defined as

$$B = (W_{CH_3})/(1 - W_{CH_3}) \qquad (4)$$

where W_{CH_3} is the weight fraction of CH_3 units. The VI typically increases with decreasing branch ratio,[8] but the reason for this behavior is not well understood. Linear alkanes have the lowest possible branch ratios and tend to have high VI.[9] Linear alkanes make poor lubricants, however, because they have high pour points. Some degree of branching is required to lower pour points, but too much branching will increase the branch ratio and lead to a lower VI. Beyond the gross branch ratio concept, most other structure−property relations for PAOs rely on empiricism and intuition. It would clearly be beneficial to have a detailed understanding of how the number, length, and relative position of branches on a PAO molecule will impact the
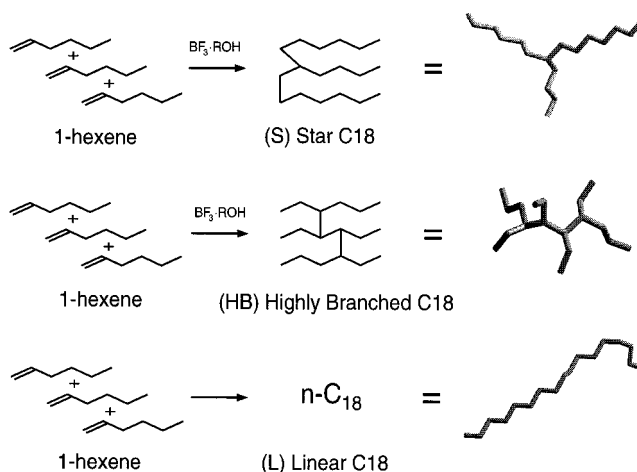
Figure 1. The three different molecular structures simulated. Their three-dimensional structures are also shown.

performance properties of that molecule as a lubricant. Examining this relationship experimentally is difficult not only in terms of time and expense, but also because synthesizing and purifying monodisperse samples is a huge challenge.

Molecular simulations, on the other hand, allow one to compute macroscopic properties of compounds with a well-defined architecture. Through this approach, there is hope that the effect of specific structural features can be deduced in an unambiguous manner. Molecular simulations have been shown to accurately reproduce experimental properties of hydrocarbon fluids, such as vapor−liquid phase equilibria[10,11] and the rheological properties of hydrocarbons. An extensive (but not comprehensive) listing of previous alkane rheology simulations may be found in a recent paper from our group.[12] Most of these works have focused on linear alkanes. A smaller number of studies have been conducted on branched species.[13−33] To our knowledge, only one group has performed molecular simulations on realistic PAO molecules.[18,23] This work, however, was focused on the conformational properties of typical PAO molecules and no viscosity computations were performed. Recently, the same group performed nonequilibrium molecular dynamics (NEMD) simulations on eicosane isomers to study the effect of side chains on fluid rheology.[32] As far as viscosity−temperature characteristics are concerned, we are aware of only one previous molecular simulation study in which the VI of the squalane molecule was calculated.[29] We should also mention the interesting work done by Mondello, Grest, Silbernagel, and Garcia,[20] in which they discuss the effect of branching density on the activation energy for diffusion. It is difficult to draw many firm conclusions from these studies, given that each had different objectives and different force fields were used to represent the fluid. What is clear, however, is that chain architecture does have an impact on the viscosity and diffusivity of the fluid, and simulations can compute these quantities with fair to good accuracy.

In the present work, we use equilibrium and nonequilibrium molecular dynamics (EMD and NEMD, respectively) to shed light on the way in which the architecture of model PAO molecules impacts performance properties. Three different 1-hexene trimer isomers are investigated (see Figure 1). These molecules represent three extreme situations. The first molecule under consideration is a starlike C_{18} alkane (7-butyl-tetradecane, designated "S"), which is produced from the trimerization of 1-hexene with no isomerization. The second molecule is a highly branched C_{18} alkane (4,5,6,7-tetraethyl-decane, designated "HB"), which undergoes a high degree of isomerization during

Impact of Molecular Architecture on Lubricants

J. Phys. Chem. B, Vol. 103, No. 49, 1999 **10783**

TABLE 1: Potential Energy Functions and Parameters for the TraPPE United Atom Model

nonbonded interactions	type	σ [Å]	ϵ/k_B [K]
$V_{LJ} = 4\epsilon_{ij}[(\sigma_{ij}/r_{ij})^{12} - (\sigma_{ij}/r_{ij})^6]$	CH_3	3.75	98
	CH_2	3.95	46
	CH	4.68	10

bond stretching	type	k_b/k_B [K/Å^2]	r_0 [Å]
$V_b = \frac{1}{2}k_b(r - r_0)^2$	CH_x-CH_y	452 900	1.54

bond-angle bending	type	k_θ/k_B [K/rad^2]	θ_0 [deg]
$V_\theta = \frac{1}{2}k_\theta(\theta - \theta_0)^2$	$CH_x-CH_2-CH_y$	62 500	114
	$CH_x-CH-CH_y$	62 500	112

torsion potential	type	a_0/k_B [K]	a_1/k_B [K]	a_2/k_B [K]	a_3/k_B [K]
$V_\phi = a_0 + a_1(1 + cos\phi)$	$CH_x-CH_2-CH_2-CH_y$	0.0	355.03	−68.19	791.32
$\quad + a_2(1 - cos2\phi)$	$CH_x-CH-CH_2-CH_y$	−251.06	428.73	−111.85	441.27
$\quad + a_3(1 + cos3\phi)$	$CH_x-CH-CH-CH_y$	−251.06	428.73	−111.85	441.27

oligomerization. Finally, a linear C_{18} molecule (*n*-octadecane, designated "L") is also simulated as an extreme situation of an alkane with no branches at all. The simulated molecules are of the same degree of polymerization to isolate the effect of the skeletal structure on macroscopic properties. Although PAO fluids produced from 1-decene are most often used in synthetic motor oils, PAOs from 1-hexene were chosen for this work. Lubricants derived from 1-hexene are used in more specialized applications where low viscosity is required. From a computational standpoint, the low viscosity of these fluids makes the calculations less demanding than would be the case for larger molecules. The 1-hexene trimers are still large enough, however, to exhibit behavior characteristic of synthetic lubricants. The choice of trimers is justified by the fact that low viscosity PAO oils produced commercially using the $BF_3 \cdot ROH$ catalyst (R is typically a short chain such as C_4) are composed mainly of trimers, with small amounts of dimers, tetramers and pentamers.[5,6,34]

2. Simulation Methods and Models

NEMD and EMD were used to compute the dynamic properties of the PAO fluids. The methods, equations of motion, and algorithmic details are described in a previous paper[12] and have also been treated extensively in several excellent references.[35−37] Here, we summarize some of the essential features of our simulations.

NEMD simulations using the Sllod algorithm[36] were used to compute the viscosity and study the effect of shear rate on rheological properties under Couette shear flow conditions. Simulations were performed at a variety of shear rates, and the shear viscosity was found from the constitutive equation

$$\eta(\dot{\gamma}) = \frac{-\langle P_{xz}\rangle}{\dot{\gamma}} \quad (5)$$

where η is the shear viscosity, $\dot{\gamma}$ is the shear rate, P_{xz} is the xz component of the pressure or stress tensor **P**, x is the direction of the flow, and z is the direction normal to the flow. The pressure tensor was computed with the virial theorem:

$$PV = \sum_i \frac{\mathbf{p}_i\mathbf{p}_i}{m_i} + \sum_i \mathbf{r}_i\mathbf{F}_i \quad (6)$$

where $\mathbf{r}_i$ is the position vector of particle i, $\mathbf{p}_i$ is the momentum vector of i measured with respect to the streaming velocity, m_i is the mass, and $\mathbf{F}_i$ is the force on particle i. The Newtonian viscosity can be obtained from an extrapolation of the viscosity

at $\dot{\gamma} \rightarrow 0$. EMD simulations were used to compute dynamic and static properties of the molecules at equilibrium conditions.

The simulations were carried out in the isothermal−isobaric (NPT) ensemble. A Nosé−Hoover chain (NHC) thermostat of length $M = 5$, combined with a Nosé−Hoover barostat was employed to maintain conditions of constant temperature and pressure.[38]

The use of extended system dynamics enables the viscosity to be computed in an alternative (but equivalent) manner to eq 5. At zero shear (EMD case), a conserved quantity $\mathcal{H}$ exists, which is the Hamiltonian of the extended system. In the NEMD simulations, the quantity $\mathcal{H}$ is no longer conserved, but instead increases linearly with time. In this case, it can easily be shown that

$$\frac{d\mathcal{H}}{dt} = -P_{xz}\dot{\gamma}V = \eta\dot{\gamma}^2 V \quad (7)$$

A plot of $\mathcal{H}$ versus simulation time t results in a straight line, the slope of which is equal to the viscous heat dissipation. Using eq 7, the viscosity η can easily be found. The two methods (eqs 5 and 7) are formally equivalent, although the second approach can sometimes be easier to estimate from a numerical simulation. More detailed analysis is required, however, before definite conclusions can be reached as to whether the use of eq 7 offers any advantage over eq 5 in computing the viscosity from NEMD simulations. At the very least, eq 7 can be used to provide a consistency check for the simulations. We have verified for the long simulations reported here that both approaches give the same result (within statistical accuracy).

The united atom transferable potentials for phase equilibria (UA-TraPPE) force field was used to represent the hydrocarbons.[39,40] This force field has been optimized for phase behavior prediction and has been shown to reproduce accurately the liquid−vapor coexistence curve and predict the critical properties for several linear and branched alkanes. The potential energy functions and parameters are listed in Table 1. Bond stretching, bond bending, torsional rotation, and van der Waals nonbonded interactions were all taken into account. Nonbonded intermolecular interactions were modeled with a pairwise Lennard−Jones (LJ) potential. Intramolecular nonbonded interactions for sites separated by more than three bonds were also described by a LJ potential. For interactions between different groups a geometric combining rule was used, so that $\epsilon_{ij} = (\epsilon_{ii}\epsilon_{jj})^{1/2}$ and $\sigma_{ij} = (\sigma_{ii}\sigma_{jj})^{1/2}$.

To speed the calculations, the reversible Reference System Propagator Algorithm (rRESPA) multiple time-step method was used to integrate the equations of motion.[38,41] As in our previous work,[12] the Liouville operator was separated in such a way so

TABLE 2: Densities (ρ), Kinematic Viscosities (ν), and Simulation Run Lengths (t_{run}) at Different Shear Rates ($\dot\gamma$) from NEMD Simulations of the Three PAO Molecules at the Two State Points Studied[a]

	40 °C, highly branched (HB)			40 °C, star (S)			40 °C, linear (L)		
$\log(\dot\gamma[1/s])$	ρ [g/cm³]	ν [cSt]	t_{run} [ns]	ρ [g/cm³]	ν [cSt]	t_{run} [ns]	ρ [g/cm³]	ν [cSt]	t_{run} [ns]
9.125	0.8132(6)	3.904(291)	4.5	0.7883(2)	2.201(191)	5.25	0.7851(3)	2.370(273)	8.0
9.250	0.8129(2)	4.224(278)	4.55	0.7884(4)	2.287(328)	5.85	0.7854(5)	2.647(153)	11.4
9.375	0.8126(4)	4.131(176)	5.4	0.7868(3)	2.216(157)	5.4	0.7853(5)	2.137(110)	8.0
9.500	0.8124(3)	3.998(133)	4.7	0.7883(4)	2.436(120)	4.7	0.7870(5)	2.334(70)	10.0
9.750	0.8098(5)	2.935(134)	3.5	0.7877(2)	2.067(41)	3.5	0.7865(7)	1.895(80)	3.5
10.00	0.8054(4)	2.393(50)	2.0	0.7856(4)	2.041(43)	2.0	0.7896(9)	1.530(76)	2.0
10.25	0.8003(6)	1.740(35)	1.2	0.7813(7)	1.428(36)	1.2	0.7861(6)	1.106(34)	1.2
10.50	0.7913(10)	1.242(19)	0.9	0.7731(6)	1.068(12)	0.9	0.7783(7)	0.834(20)	0.8
10.75	0.7781(11)	0.860(14)	0.6	0.7598(8)	0.764(15)	0.6	0.7658(8)	0.568(12)	0.5
11.00	0.7553(8)	0.573(5)	0.6	0.7433(8)	0.534(7)	0.6	0.7496(5)	0.437(8)	0.5

	100 °C, highly branched (HB)			100 °C, star (S)			100 °C, linear (L)		
$\log(\dot\gamma[1/s])$	ρ [g/cm³]	ν [cSt]	t_{run} [ns]	ρ [g/cm³]	ν [cSt]	t_{run} [ns]	ρ [g/cm³]	ν [cSt]	t_{run} [ns]
9.250	0.7737(5)	1.407(197)	5.4	0.7486(3)	0.963(124)	7.8	0.7448(4)	1.168(108)	11.4
9.375							0.7452(4)	1.147(100)	8.0
9.500	0.7732(4)	1.410(60)	7.2	0.7482(2)	1.026(108)	4.0	0.7447(3)	1.305(62)	10.0
9.625							0.7447(4)	1.057(60)	8.0
9.750	0.7732(3)	1.352(54)	6.0	0.7476(3)	1.034(75)	3.0	0.7455(4)	1.058(46)	7.0
10.00	0.7723(4)	1.170(45)	1.5	0.7472(6)	0.954(43)	1.5	0.7478(7)	1.009(42)	2.0
10.25	0.7692(12)	1.118(44)	1.0	0.7447(8)	0.902(42)	1.0	0.7456(6)	0.889(21)	1.2
10.50	0.7620(12)	0.874(23)	0.6	0.7408(9)	0.742(23)	0.6	0.7439(7)	0.693(29)	0.8
10.75	0.7501(12)	0.705(14)	0.4	0.7333(7)	0.630(21)	0.4	0.7353(7)	0.518(11)	0.5
11.00	0.7307(8)	0.512(7)	0.4	0.7182(9)	0.463(8)	0.4	0.7194(7)	0.407(6)	0.5

[a] The numbers in the parentheses represent the statistical uncertainties in the last reported digits, computed from block averaging.

that fast modes (bond stretching, bond-angle bending, and torsional rotation) were integrated with a small time step δt. The slow modes (intermolecular and intramolecular nonbonded LJ forces) were integrated with a larger time step $\Delta t = n\delta t$, where n is an integer. Consequently, the number of computationally expensive LJ force evaluations were reduced for a given overall simulation time. A multiple time-step scheme was also used to integrate the motion of the NHC accurately. To reduce the computational overhead associated with the application of the NHC, a sixth-order symplectic integration scheme was employed.[38] The extension of the algorithm to integrate the NPT−Sllod equations of motion is described in detail in ref 42.

3. Simulation Details

The NEMD simulations were carried out at 40 and 100 °C over a range of shear rates. The EMD simulations were performed at 40, 60, 80, and 100 °C. The pressure was kept constant at 20 bar in all runs. A small time step of $\delta t = 1$ fs was used to integrate the fast modes and a large time step of $\Delta t = 5$ fs was used for the slow modes. These time-step sizes were chosen through a trial-and-error optimization procedure; smaller time steps yielded essentially the same results. For the NEMD runs, the same size time steps were used for all different shear rates. No significant differences in the calculated properties were observed by using smaller time steps, even for the high shear rate runs. The thermostat and barostat time constants were 0.1 and 2.5 ps, respectively. The LJ potential was truncated at 10 Å, and long-range corrections were included in the calculation of the intermolecular energy and pressure. Larger cutoff distances were also tested, but no appreciable differences in the results were observed. The length of the simulation runs varied from 2 to 8 ns for the EMD runs, and from 0.4 to 11.4 ns for the NEMD runs. The simulations were performed using 60 molecules in the periodic box. For the EMD case, however, multiple runs were performed at each state point from different starting configurations to improve statistics. For the EMD runs
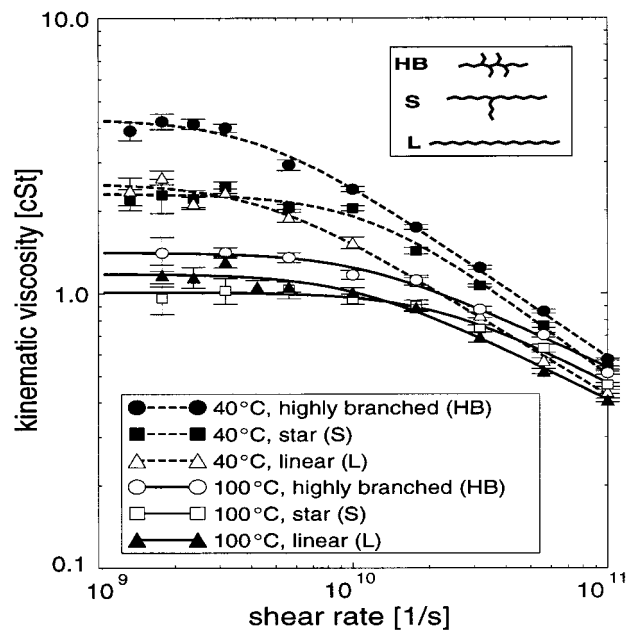
Figure 2. Kinematic viscosity (ν) versus shear rate ($\dot\gamma$) from NEMD simulations at 40 and 100 °C. The lines are fits using the Carreau model (eq 8).

at 40 and 100 °C, the results were averaged over four different runs, whereas at 60 and 80 °C, three runs were averaged.

4. Results and Discussion

4.1. Viscosity. Table 2 lists the kinematic viscosities of the fluids at 40 and 100 °C computed from the NEMD simulations, along with the calculated densities and the simulation lengths for each run. The kinematic viscosity ν is defined as the ratio $\nu = \eta/\rho$, where η is the shear viscosity as computed from eq 5, and ρ is the density. In Figure 2 the computed values of the viscosity are plotted as a function of shear rate. The data are fitted with the Carreau model[43]

Impact of Molecular Architecture on Lubricants

J. Phys. Chem. B, Vol. 103, No. 49, 1999 **10785**

$$\nu = \frac{\nu_0}{[1 + (\lambda\dot{\gamma})^2]^p} \tag{8}$$

where the parameters ν_0, p, and λ have the following physical meaning. In the limit of zero shear rates ($\dot{\gamma} \rightarrow 0$) the viscosity plateaus off to its Newtonian value ν_0. At high shear rates ($\dot{\gamma} \rightarrow \infty$) the viscosity decreases (shear-thinning), and the viscosity versus shear rate curve approaches a power law $\nu \propto \dot{\gamma}^{-2p}$, where $2p$ is the slope of the log ν versus log $\dot{\gamma}$ curve. The parameter λ is a characteristic time constant, which approximately equals the inverse of the shear rate corresponding to the transition from the Newtonian to non-Newtonian regime. The parameters from the Carreau fit are listed in Table 3.

From Figure 2 it is evident that the HB molecule has the largest viscosity of the three fluids at every shear rate. The star molecule has the smallest Newtonian kinematic viscosity. A comparison between the star and the linear molecule reveals some interesting results. Although the star molecule has a smaller Newtonian viscosity, at high shear rates the behavior is reversed; the linear molecule shear-thins more dramatically than the star. This result agrees qualitatively with experimental findings for star and linear unentangled polymers.[44] Similar behavior has been observed in the simulations of Evans and co-workers for linear and star tridecane molecules.[14] The reason for this behavior is that the linear molecules tend to align easily with the shear flow, which results in shear-thinning.[12] The star molecule, on the other hand, is more resistant to alignment (i.e., shear-thinning), which is a highly desirable behavior for a lubricant. The shear-thinning behavior of the HB molecule is similar to the linear molecule. Both molecules start to shear-thin at almost the same shear rates, and the λ parameters from the Carreau fit are nearly identical (see Table 3). The reason for the similar shear-thinning behavior of the HB and L molecules is not obvious, and is discussed in greater detail in *Section 4.3*.

The Newtonian kinematic viscosities ν_0 at 40 and 100 °C as predicted from the Carreau fit (see Table 3), are plotted in Figures 3a and b using the Walther and Eyring expressions, respectively. The computed values of the viscosity numbers (VN) and activation energies (E) from the Eyring model are also shown. We were able to find experimental viscosity data only for the linear C_{18}. The literature values of the kinematic viscosity of n-C_{18} at 40 and 100 °C are 3.9 and 1.6 cSt, respectively.[45] As was also the case in our previous study,[12] the present work indicates that the TraPPE force field model tends to consistently under predict the experimental viscosity, particularly at low temperatures. However, the model does a better job predicting *relative changes* in viscosity with temperature, as indicated by the excellent agreement between the experimental VN value of 103 and the simulated VN of value 101. The agreement between the experimental Eyring activation energy $E = 1743$ K and the computed value $E = 1474$ is fair. These results indicate that even when simulations do not accurately match absolute values of a given quantity they can be fairly accurate at capturing relative changes in a quantity, which is the main interest here. In Figures 3a and 3b it is shown that the HB molecule exhibits the largest decrease in viscosity in moving from 40 to 100 °C. This molecule has the smallest VN and the highest activation energy E of all the fluids. The linear molecule exhibits the best viscosity−temperature dependence, whereas the star molecule exhibits intermediate performance properties. These results are consistent with the empirical observation that a high branch ratio gives a low VN. Importantly, the viscosity and VN of the star molecule do not differ much

TABLE 3: Parameters of the Carreau Model (eq 8) from Fitting the NEMD Results[a]

PAO molecule	T [°C]	ν_0 [cSt]	λ [ps]	p
highly branched (HB)	40	4.324 ± 0.148	231 ± 7	0.319 ± 0.010
	100	1.413 ± 0.035	89 ± 2	0.221 ± 0.004
star (S)	40	2.307 ± 0.097	84 ± 3.5	0.356 ± 0.014
	100	1.012 ± 0.025	46 ± 1.5	0.248 ± 0.007
linear (L)	40	2.523 ± 0.099	224 ± 9	0.286 ± 0.011
	100	1.183 ± 0.042	97 ± 4	0.233 ± 0.009

[a] The statistical uncertainties are from the standard error of the fit.
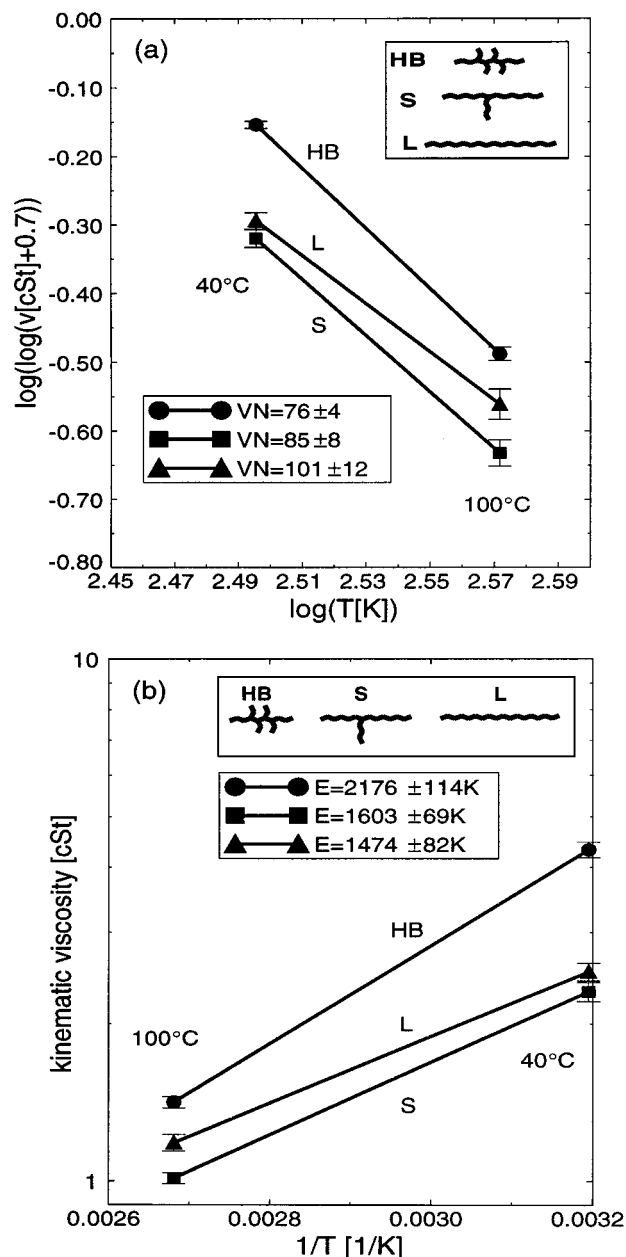
Figure 3. Temperature dependence of the Newtonian kinematic viscosity ν_0 using (a) the Walther equation, and (b) the Eyring model. The statistical uncertainties shown for the viscosity numbers (VN) and Eyring activation energies (E) were computed from propagation of errors using the defining eqs 1, 2, and 3, respectively.

from the linear species, but the star molecule has a much lower pour point than the linear molecule (trimers of 1-hexene have pour points of < -55 °C,[5] whereas n-C_{18} has a pour point near room temperature). These results indicate that the star molecule should have the best overall lubricant properties, which agrees

TABLE 4: Density (ρ), Square Radius of Gyration (R_g^2), Overall Torsion Angle Rotational Diffusivity (D_ϕ), Rotational Relaxation Time (τ_1), and Self-Diffusion Coefficient (D_s) Values Computed from EMD Runs[a]

PAO	T [°C]	ρ [g/cm^3]	R_g^2 [Å^2]	D_ϕ [10^{-4} rad^2/ps]	τ_1 [ps]	D_s [10^{-10} m^2/s]	t_{run} [ns]
HB	40	0.8134(4)	10.13(1)	2.95(10)	188(3)	1.66(3)	8
	60	0.8002(6)	10.13(1)	6.32(16)	111(3)	2.71(7)	2
	80	0.7867(5)	10.14(1)	13.3(3)	73(2)	4.36(9)	2
	100	0.7738(4)	10.15(1)	21.3(4)	56(1)	6.00(6)	6
S	40	0.7879(3)	19.67(2)	228(8)	216(3)	3.13(5)	8
	60	0.7746(5)	19.52(3)	340(9)	119(3)	4.51(12)	2
	80	0.7611(6)	19.34(3)	484(11)	84(2)	7.08(16)	2
	100	0.7477(3)	19.16(2)	670(13)	70(1)	9.21(9)	6
L	40	0.7846(5)	31.24(9)	364(16)	332(8)	5.58(13)	5
	60	0.7710(4)	30.62(11)	527(18)	219(8)	8.53(30)	2
	80	0.7576(7)	30.16(11)	733(22)	153(5)	10.01(30)	2
	100	0.7451(5)	29.72(7)	970(25)	124(2)	13.04(21)	4

[a] Numbers in the parentheses represent statistical uncertainties in the last reported digits. The error used for the statistical uncertainties is defined as $\epsilon\% = (2\tau_1/N_r N t_{run})^{1/2} \times 100$,[12] where τ_1 is the rotational relaxation time of the longest axis, which can be assumed to be the longest relaxation time of the molecule, N_r is the number of different runs used, N is the number of molecules in each run, and t_{run} is the simulation length in each run. All results were averaged over $N_r = 4$ runs for 40 °C and 100 °C, and $N_r = 3$ runs for 60 °C and 80 °C and t_{run} as shown in the table, except for the D_ϕ values which were averaged over three runs of 2 ns each at all different temperatures.

with past experimental findings.[9] Actual synthetic lubricants do in fact contain a large fraction of "star-shaped" PAO molecules.[8]

4.2. Other Dynamic Properties. EMD simulations were also performed to study the equilibrium properties of the molecules. Among several dynamic and static properties studied using EMD, the dynamics of the torsion angle rotation seems to be most responsible for the observed high viscosities and low VN of molecules with high branch ratios. To quantify this, a rotational diffusion coefficient D_ϕ can be defined as.[46]

$$D_\phi = \frac{1}{2} \lim_{t \to \infty} \frac{d}{dt} \langle (\phi(t) - \phi(0))^2 \rangle \qquad (9)$$

In a manner analogous to the Einstein expression for self-diffusivity, D_ϕ is computed from the limiting slope of the mean square displacement (MSD) of the torsion angles ϕ. Care was taken so that the MSD just mentioned is unbounded and that at long times yields a linear function. To achieve this, an unfolding routine is applied to $\phi(t)$ at each time step. When the angle $\phi(t)$ has rotated a complete cycle, a value of 2π is added or subtracted to $\phi(t)$. We assume that the torsional rotation diffusivity D_ϕ is a good measure of how fast the torsion angles rotate and of the rate of trans−gauche and gauche−gauche transitions.

Values of D_ϕ averaged over each torsion angle for each molecule are listed in Table 4. Other properties listed in Table 4 will be discussed later. In Figure 4 the averaged D_ϕ values for each molecule are shown in an Arrhenius plot. The D_ϕ values of the HB molecule are orders of magnitude smaller than the D_ϕ values of the other two molecules. The torsion angle rotational dynamics of the HB molecule are extremely slow, whereas the rotation of the torsion angles in the L molecule is quite fast. An interesting observation from Figure 4 is that D_ϕ of the HB molecule has much higher Arrhenius activation energy than for the other molecules; that is, the dynamics of rotation of the torsion angles are more temperature dependent for the HB molecule than for the S or L, which is in agreement with what was observed in Figure 3 for viscosity. In addition, the L molecule (which has the best viscosity−temperature dependence) has the smallest Arrhenius activation energy for D_ϕ.
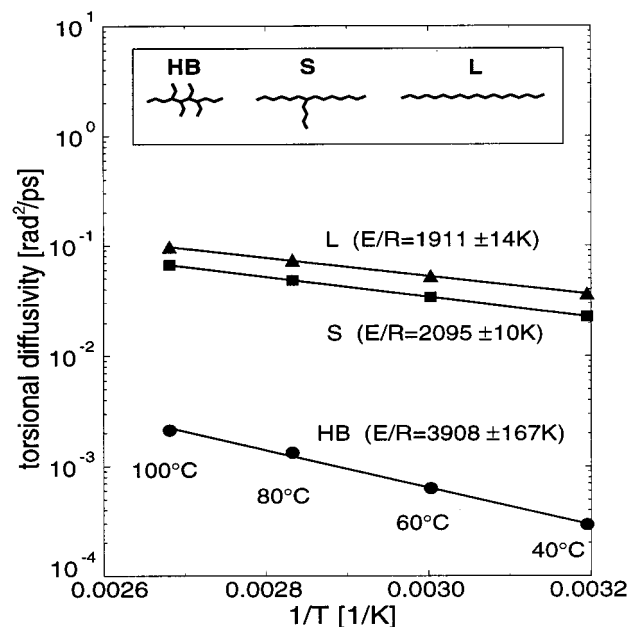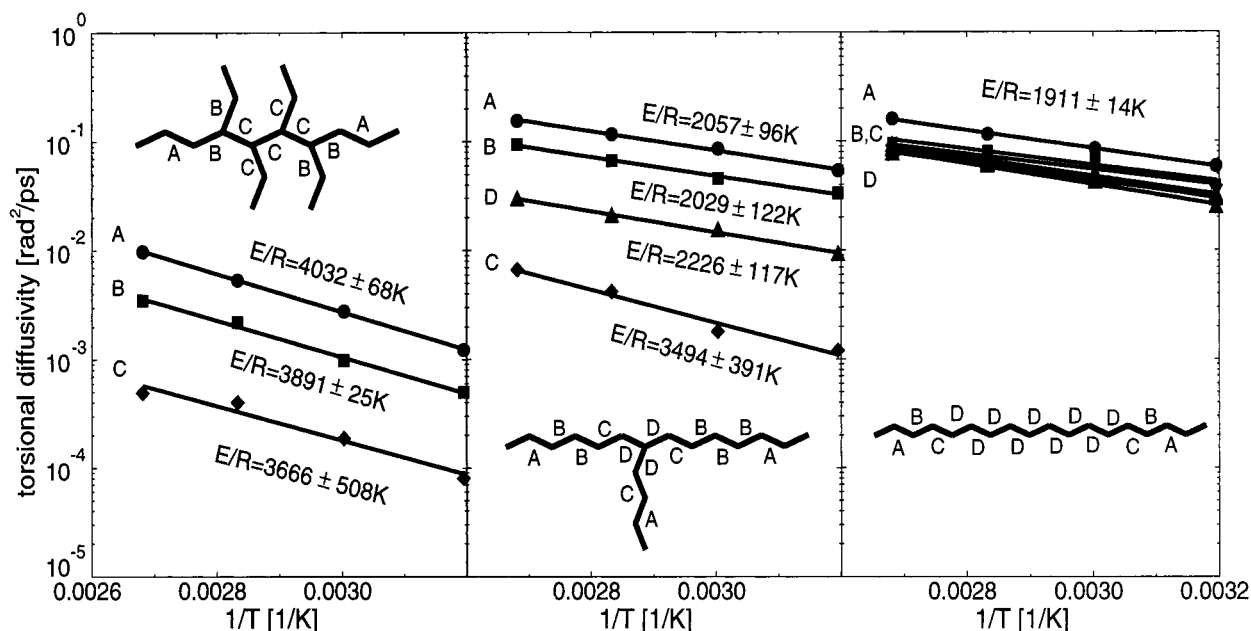

Figure 4. Temperature dependence of the overall torsion angle diffusivity D_ϕ. The straight lines are fits using the Arrhenius expression $A \exp(-E/RT)$. The statistical uncertainties shown for the activation energies are the uncertainties from the fit.

A study of the torsional rotation for individual angles in each molecule can explain in more detail the impact of branching on VN. As can be seen in Figure 5, several regimes of D_ϕ can be identified, each corresponding to different torsion angle locations along the molecule. The linear molecule exhibits fast torsion angle rotation for all angles. Angles at the chain ends (angles A) exhibit slightly higher values of D_ϕ than angles in the interior of the chain (B, C, D). D_ϕ is nearly independent of position after the third angle from the end.

For the star molecule four different regimes were observed. Angles at the chain ends (angles A) and on the branches (angles B) have the highest values of D_ϕ. These values are about the same magnitude as the D_ϕ values of the linear chain. The angles close to the branch point (C and D), on the other hand, have much slower torsional rotation dynamics. Intramolecular steric effects caused by the interaction of the bulky "arms" of the star inhibit rotation about angles C and D.

For the HB molecule, D_ϕ values are much smaller than for the other molecules. The angles in the interior of the HB molecule have extremely slow dynamics of rotation. The chain ends (angles A) rotate faster, but still the rotation is much smaller than what is seen for the chain ends of the other two molecules. Almost all angles are close to a branch point and it is hard for those angles to rotate because of steric constraints.

As far as the dependence of D_ϕ on temperature, it is observed that the dynamics of angles close to a branch point exhibit much higher Arrhenius activation energies than those angles far from a branch point. This large difference in the activation energies seems to be the most important factor as to why the HB molecule has the smallest VN, whereas the L molecule, which has no branches at all, has the highest VN. We believe this important factor provides a molecular-level reason for the empirical observation that a low branch ratio corresponds to a high VI (or VN). Molecules with a high degree of intramolecular mobility should exhibit a higher VN than molecules with low intramolecular mobility. For PAOs, this statement suggests that molecules with sparse, long, and widely spaced branches will have a higher VN than those with many short and closely spaced

Impact of Molecular Architecture on Lubricants

*J. Phys. Chem. B, Vol. 103, No. 49, 1999* **10787**

Figure 5. Temperature dependence of the torsional diffusivity D_ϕ for different angles in each molecule. The angles of the different A, B, C, or D regimes are torsion angles around a central bond represented with the same letter, as shown. The values reported are the average values over all angles in each regime. The straight lines are fits using the Arrhenius expression $A \exp(-E/RT)$. The statistical uncertainties shown for the activation energies are the uncertainties from the fit.

branches. It also suggests that other strategies that lower conformational rotation barriers, such as the addition of heteroatoms to the chain backbone, may also increase the VN. The observations just presented are consistent with the results of the work done by Mondello et al.[20] In this work, the authors analyze diffusion for both a "star" and "double star" molecule and compare this with both a linear molecule and a quasi-linear molecule (squalane). They mention evidence for correlation between decreased dynamic flexibility and increased temperature dependence of self-diffusivity.

Another important dynamic property is the rotational relaxation rate of the longest axis of the molecules. This property gives an indication of how fast the molecules "tumble". A relaxation time τ_1 associated with this process can be computed from the decay of the rotational autocorrelation function $\langle \mathbf{e}_1(0) \cdot \mathbf{e}_1(t) \rangle$, where $\mathbf{e}_1$ is the unit vector of the longest axis of the molecule. The longest axis of the molecule has the same direction as the principal axis of an ellipsoid inertially equivalent to the molecule. The unit vector $\mathbf{e}_1$ is found from the eigenvector corresponding to the smallest eigenvalue of the averaged tensor of inertia of each molecule.[14] The relaxation time τ_1 was computed with the following expression

$$\tau_1 = \int_0^\infty \langle \mathbf{e}_1(0) \cdot \mathbf{e}_1(t) \rangle \, dt = \int_0^\infty e^{-(t/\tau)^\beta} \, dt \quad (10)$$

where the autocorrelation function has been fitted to the Kohlraush−Williams−Watt (KWW) expression.[47] A complete listing of computed relaxation times is given in Table 4. In Figure 6 the rotational relaxation time τ_1 is shown in an Arrhenius plot. The HB molecule has the highest activation energy for tumbling, whereas the L molecule the smallest. This result is consistent with what has been seen so far for temperature dependence of the viscosity and D_ϕ. A comparison of the *magnitude* of τ_1 for each molecule, however, reveals a more complicated picture. The HB molecule, which has the smallest diffusivity (see Table 4 and Figure 7) and the largest viscosity, has the fastest rate of tumbling (i.e., smallest τ_1). This result is counterintuitive at first glance. Polymer theories such
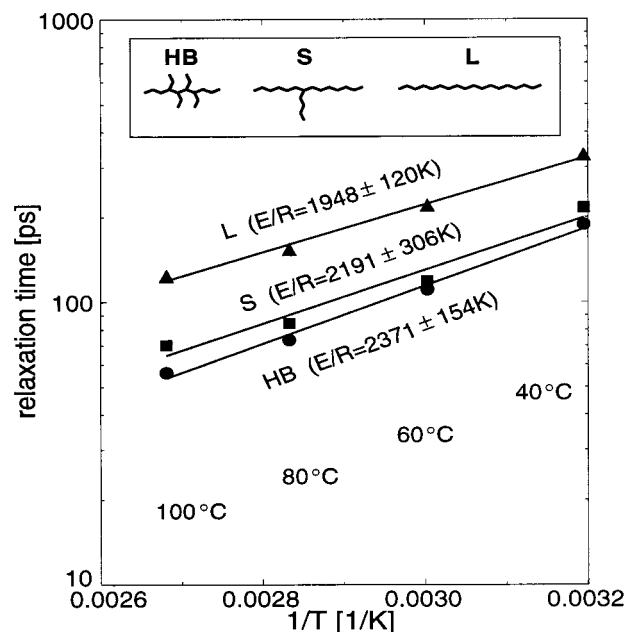
Figure 6. Temperature dependence of the rotational relaxation time τ_1. The straight lines are fits using the Arrhenius expression $A \exp(E/RT)$. The statistical uncertainties shown for the activation energies are the uncertainties from the fit.

as the Rouse theory[48] predict that the viscosity is directly proportional to τ_1 and the diffusivity is inversely proportional to τ_1. The opposite is true here. The reason for the discrepancy is that the HB molecule has the smallest radius of gyration of the three molecules under study. This small radius enables it to rotate faster while still exhibiting a high viscosity and low diffusivity. In fact, the Rouse theory also predicts that $\tau_1 \propto R_G^2$, which is roughly true for the present case. We should point out that the Rouse theory has been shown in recent simulation work on *n*-alkanes[49] to provide the proper scaling for viscosity and diffusivity with τ_1. The present work serves as a reminder, however, that great caution must be taken when applying
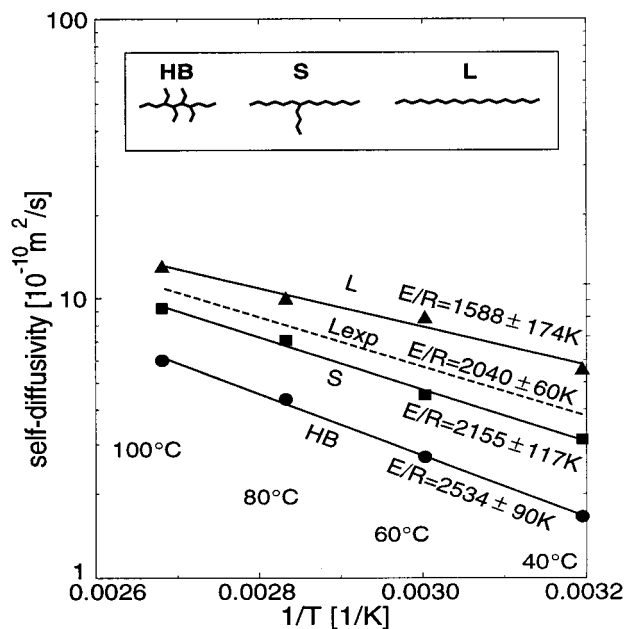
Figure 7. Temperature dependence of the self-diffusion coefficient D_s. The straight lines are fits using the Arrhenius expression A exp-$(-E/RT)$. The statistical uncertainties shown for the activation energies are the uncertainties from the fit. The dashed line is experimental data for n-C_{18} from ref 50.

theories of this type to branched oligomeric species such as lubricant molecules. For the HB molecule, the rotational dynamics of the dihedral angles appears to be the most important factor in determining the trends in viscosity and diffusivity; τ_1 seems to be of secondary importance.

The self-diffusion coefficient D_s was also computed from EMD simulations. Values of D_s are listed in Table 4, and an Arrhenius plot of the self-diffusion coefficients is shown in Figure 7. These results were obtained by calculating the long-time slope of the mean square displacement of the center of mass of each chain and applying the Einstein equation for diffusion.[35]

$$D_s = \frac{1}{6} \lim_{t \to \infty} \frac{d}{dt} \langle (\mathbf{r}(t) - \mathbf{r}(0))^2 \rangle \tag{11}$$

In Figure 7 the experimental curve for the linear C_{18} (Lexp) is also shown.[50] The experimental diffusivity values are smaller by 30−15%, as we move from low to high temperatures. As has also been discussed in refs 12 and 51, the TraPPE force field model tends to give slightly faster dynamics (higher diffusivity, lower viscosity) than experiment. As was seen with the trend in viscosity, the HB molecule has the highest Arrhenius activation energy for diffusion, and the L molecule has the lowest. The HB molecule also has the smallest diffusivity, which is in agreement with its high viscosity. Comparing the L and S molecules is a bit more complicated. Whereas the L molecule had a higher Newtonian viscosity than the S molecule, the L molecule also has a higher value of D_s and D_ϕ than the S molecule. The differences in architecture of these two molecules with the same number of carbon atoms results in a complicated interplay between the different dynamic phenomena. Apparently, there are several competing factors that govern the resulting diffusivity and viscosity; no simple rule is evident that would enable one to directly predict how the architecture of the molecule will impact its transport properties. Nevertheless, the current results do indicate that the dependence of the dynamic properties on temperature is strongly related to the magnitude of the activation barriers for intramolecular motion.
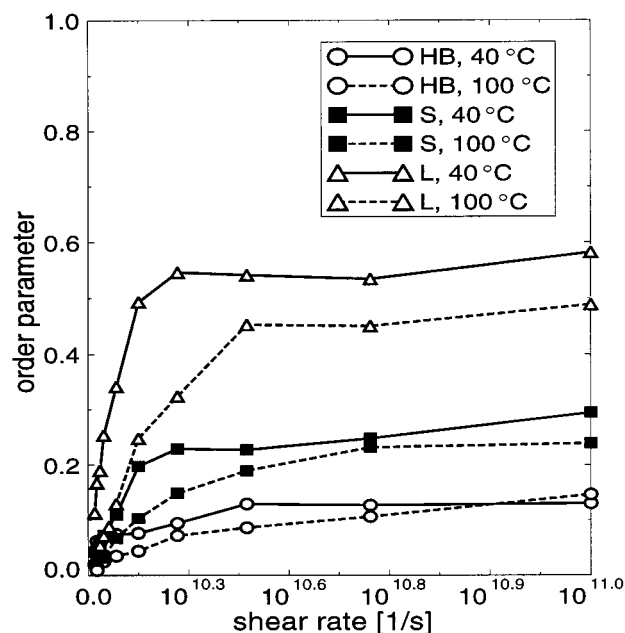
Figure 8. Order parameter (λ) versus shear rate ($\dot{\gamma}$) from NEMD simulations.

4.3. Effect of Shear Rate. In *Section 4.1* we saw that the star molecule shear-thins at rates higher than the other two molecules (see Figure 2). This property is desirable for lubricants. The star PAO resists viscosity loss and can provide good lubrication under conditions of high shear rates. Previous studies on mainly linear alkanes[12,14,33,52] have shown that the microscopic mechanism responsible for shear-thinning is the increased alignment and orientational ordering of the molecules under shear. To study the structural order of the fluid under shear, we have used the order tensor defined as[12]

$$\mathbf{S} = \frac{3}{2} \left\langle \frac{1}{N} \sum_{i=1}^{N} \left(\mathbf{e}_{1i} \, \mathbf{e}_{1i} - \frac{1}{3} \mathbf{I} \right) \right\rangle \tag{12}$$

where, $\mathbf{e}_{1i}$ is the unit vector along the longest axis of molecule i (defined from the eigenvector corresponding to the smallest eigenvalue of the moment of inertia of molecule i), and $\mathbf{I}$ is the unit tensor. The order tensor is a measure of the anisotropy of the average inertia tensor of a flexible molecule caused by the shear field. The largest eigenvalue λ of the order tensor is called the order parameter, and the eigenvector corresponding to the largest eigenvalue λ has the same direction as the principal axis of an orientationally equivalent ellipsoid to the fluid. The value of the order parameter λ can vary from zero for randomly oriented (disordered) fluid at equilibrium to unity for perfect orientational alignment. It is interesting to examine if the relationship between orientational alignment and shear-thinning observed with linear alkanes holds true for branched alkanes as well.

In Figure 8, the order parameter λ is plotted as a function of the shear rate. The general trend is that λ increases with shear rate, indicating an increased orientational ordering and more pronounced alignment of the molecules as shear rates increase. The shear ordering is higher at the lower temperature (40 °C) for all different molecules. The L molecule exhibits more pronounced order than the S molecule, with λ rising more rapidly with shear rate. This result matches the shear-thinning behavior observed in Figure 2, and is consistent with the previous studies that explained shear-thinning in terms of alignment. The situation is more complicated for the HB

Impact of Molecular Architecture on Lubricants
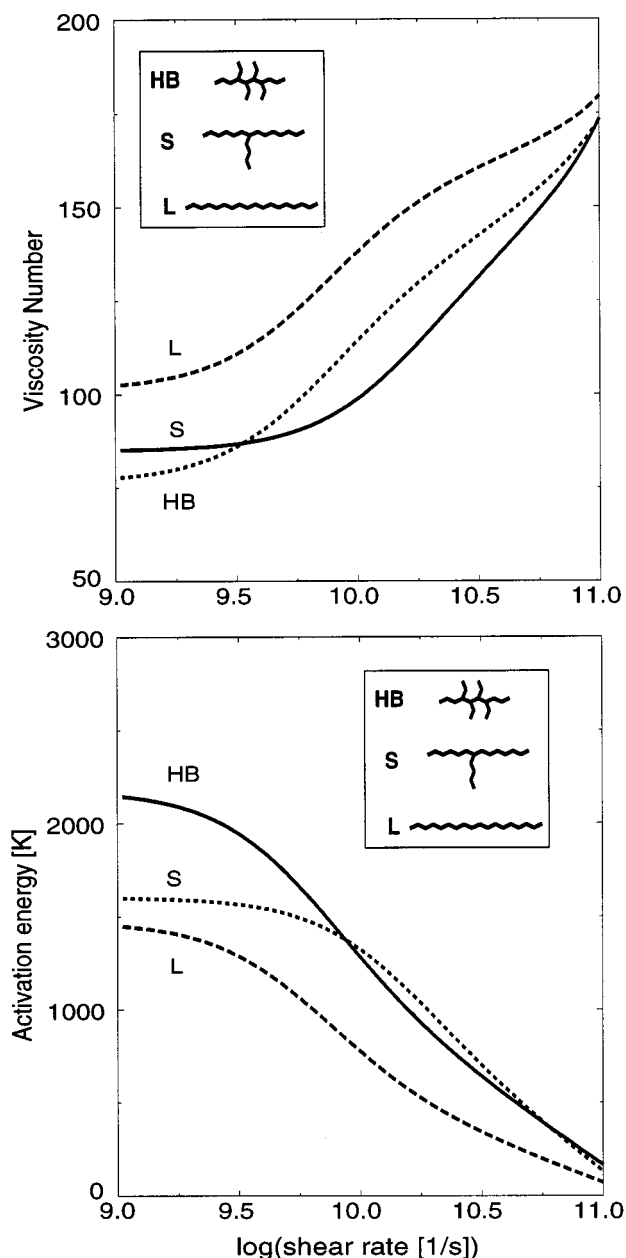
J. Phys. Chem. B, Vol. 103, No. 49, 1999 **10789**

molecule, however. The HB molecule exhibits very little ordering due to shearing, despite the fact that its shear-thinning behavior is similar to that of the easily aligned L molecule. Apparently, the relationship between alignment with the flow field and shear-thinning breaks down for more "globular" species such as the HB molecule.

In a previous study by us[12] on mixtures of short and long *n*-alkanes, it was observed that the shorter molecule had smaller values of λ, and therefore less ordering. The same trend is observed here; the HB molecule has the smallest radius of gyration and the least order, whereas the L molecule exhibits the greatest alignment and largest radius of gyration. The order parameter appears to scale with the radius of gyration, but not always with the degree of shear-thinning. A more general picture as to the microscopic origin of shear-thinning may emerge by considering the relative magnitude of the forces due to the flow field and the interchain "drag" forces. When these two forces become commensurate, shear-thinning will occur. For essentially linear molecules, interchain forces decrease as the chains align and reduce the number of overlapping segments. For highly branched molecules, it takes very high flow fields to distort the molecule and cause it to align. These molecules shear-thin at relatively low shear rates, however, because their more globular nature reduces the number of interchain contacts and enables them to "slide" past one another more easily. This picture may also serve to explain why the star molecule shear-thins at the highest shear rates. Even when part of its backbone aligns with the flow, one long "arm" is able to interact with one or more neighboring molecules, thereby increasing "drag" and delaying the onset of shear-thinning. This result suggests that relatively long branches are desirable to delay the onset of shear-thinning. The short branches on the HB molecule cannot interpenetrate neighboring molecules as effectively as the single long branch of the S molecule. Another possible explanation for the observed behavior is that the rate of rotation of dihedral angles for highly branched molecules increases at a faster rate with increasing shear rate than for linear or moderately branched species.

Viscosity numbers (VN) and activation energies (*E*) were also computed at various shear rates to examine the effect of shear rate on the viscosity–temperature properties of the PAO molecules. In Figure 9 plots of VN and activation energy versus shear rate are shown. The values were computed using the Carreau fit from Figure 2. The main observation is that VN increases as $\dot\gamma$ increases. Analogously, *E* decreases as $\dot\gamma$ increases. These trends reflect the fact that at high shear rates, the behavior of the fluids is dominated by the strong kinematic field rather than the thermodynamic state point. Similar behavior has been seen in simulations of *n*-hexadecane done by Chynoweth et al.,[52] where they studied the pressure and temperature effect on viscosity in the non-Newtonian regime.

What is more interesting though, is that there is a crossover in the VN and *E* versus $\dot\gamma$ curve for the HB and S molecules. That is, the VN of the HB molecule is actually greater than the VN of the S molecule at high shear rates. This behavior arises from the fact that the HB molecule shear-thins at smaller shear rates than the S molecule. A large increase in VN is also seen for the L molecule, which also shear-thins easily. Therefore, shear-thinning increases the VN and decreases the differences in viscosity between the two state points. We should point out, however, that the resistance to shear-thinning of the star PAO is typically a more desirable property for lubricants because it guarantees no loss in the oil's viscosity under high shear rates.

A point that needs emphasizing from the analysis just presented is that the behavior of the fluids under high shear

Figure 9. Viscosity number (VN) and Eyring activation energy (*E*) versus shear rate ($\dot\gamma$).

conditions can be very different from what is observed in the Newtonian regime. Because lubricants frequently operate at extremely high shear rates, it is important to understand how the lubricant properties will change under shear. Simulations enable one to examine this relationship quite easily, whereas the corresponding experiments under extreme conditions can be quite challenging. We should point out that the shear rates used in the simulations are large, but not completely unrealistic. Shear rates in several lubrication applications frequently fall into the 10^8 s^{-1} range or higher, which is only an order of magnitude lower than the shear rates studied here. PAOs with higher molecular weights will shear-thin at even lower shear rates than those studied here. Understanding the shear-thinning behavior of these materials is critical; simulations of the type described here can play an important role in this process.

5. Conclusions

Molecular dynamics simulations were performed to study the temperature dependence of viscosity and other dynamic proper-

ties of typical PAO fluids. The goal was to examine the role of molecular structure on rheological and lubricant performance properties. Three different hydrocarbon structures were simulated: a star-shaped C_{18}, a highly branched C_{18}, and a linear C_{18}. These structures correspond to three extreme isomer PAO molecules produced from trimerization of 1-hexene.

Computed viscosities showed fair agreement with experimental values for n-C_{18} (the only system for which data were available). Computed viscosity numbers were in excellent agreement with experiment. The HB molecule has the smallest VN and therefore exhibits the largest dependence of viscosity with temperature. On the other hand, the linear C_{18} gave the largest VN. This result confirms the empirical observation that PAO fluids with high branch ratios give lubricants with low VN and are therefore poor motor oils.

Other dynamic properties such as torsion angle rotational dynamics, rotational relaxation times, and self-diffusivity were computed from EMD simulations. The temperature dependence of these properties was investigated in terms of Arrhenius activation energies. As was the case with viscosity, the dynamics of the highly branched molecule showed the strongest dependence on temperature, whereas the linear molecule showed the weakest dependence. The simulation results indicate a strong relationship between the activation barriers for torsion angle rotation and the VN. The HB molecule had the lowest VN and exhibited extremely slow torsion angle dynamics and high rotation barriers. The linear and single-branch molecules showed much more facile torsional rotations and had higher VN. These observations suggest that strategies for improving VN should focus on ways of lowering activation energies for intramolecular motion. Long, widely spaced branches are desirable. One may also be able to substitute heteroatoms into the chain backbone to lower activation energies. The simulations suggest that bulky substituent groups that impede intramolecular motion should result in lower VN.

Finally, the effect of shear rate on the PAO properties was investigated. It was shown that high shear rates and shear-thinning increases the VN. At conditions of high shear rates, kinematics dominate thermodynamics and the behavior of the fluids is determined by the strong flow field rather than by thermal effects. It was found that molecular alignment with the flow field does not always correlate with enhanced shear-thinning, as is the case with linear alkanes. Shear-thinning appears to stem from a competition between intermolecular forces and the forces due to the flow field. Highly branched, globular molecules can readily shear-thin without showing significant alignment with the flow field. Star-type molecules can delay shear-thinning even when the main backbone shows strong alignment with the flow field, because of their "arms" interacting with neighboring molecules. This property, combined with its low pour point and high VN makes the star molecule the "best" lubricant of the three species simulated.

References and Notes

(1) ASTM D-2270−79 "Standard Viscosity Index from Kinematic Viscosity at 40 and 100 °C.", 1979.

(2) Hardiman, E. W.; Nissan, A. H. *J. Inst. Pet.* **1945**, *31*, 255.

(3) Dean, E. W.; Davis, G. H. B. *Chem. Met. Eng.* **1929**, *36*, 618.

(4) Sanchez-Rubio, M.; Heredia-Veloz, A.; Puig, J. E.; Gonzalez-Lozano, S. *Lubr. Eng.* **1992**, *48*, 821.

(5) Brennan, J. A. *Ind. Eng. Chem. Prod. Res. Dev.* **1980**, *19*, 2.

(6) Shubkin, R. L.; Baylerian, M. S.; Maler, A. R. *Ind. Eng. Chem. Prod. Res. Dev.* **1980**, *19*, 15.

(7) Henze, H. R.; Blair, C. M. *J. Am. Chem. Soc.* **1931**, *53*, 3077.

(8) Wu, M. M. High Viscosity Index Synthetic Lubricant Compositions. U.S. Patent 4,827, 064, May 2, 1989.

(9) Denis, J. *J. Synth. Lubr.* **1984**, *1*, 201.

(10) Siepmann, J. I.; Karaborni, S.; Smit, B. *Nature* **1993**, *365*, 330.

(11) Smit, B.; Karaborni, S.; Siepmann, J. I. *J. Chem. Phys.* **1995**, *102*, 2126; Smit, B.; Karaborni, S.; Siepmann, J. I. *J. Chem. Phys.* **1998**, *109*, 352.

(12) Kioupis, L. I.; Maginn, E. J. *Chem. Eng. J.* **1999**, *74*, 129.

(13) Rowley, R. L.; Ely, J. F. *Mol. Phys.* **1991**, *72*, 831.

(14) Daivis, P. J.; Evans, D. J.; Morris, G. P. *J. Chem. Phys.* **1992**, *97*, 616.

(15) Wang, Y.; Hill, K.; Harris, J. G. *Langmuir* **1993**, *9*, 1983.

(16) Mondello, M.; Grest, G. S. *J. Chem. Phys.* **1995**, *103*, 7156.

(17) Padilla, P. *J. Chem. Phys.* **1995**, *103*, 2157.

(18) Lahtela, M.; Pakkanen, T. A.; Nissfolk, F. *J. Phys. Chem.* **1995**, *99*, 10267.

(19) Lee, S. H.; Cummings, P. T. *Mol. Simul.* **1996**, *16*, 229.

(20) Mondello, M.; Grest, G. S.; Garcia, A. R.; Silbernagel, B. G. *J. Chem. Phys.* **1996**, *105*, 5208.

(21) Allen, W.; Rowley, R. L. *J. Chem. Phys.* **1997**, *106*, 10273.

(22) Lahtela, M.; Pakkanen, T. A.; Rowley, R. L. *J. Phys. Chem. A* **1997**, *101*, 3449; Lahtela, M.; Pakkanen, T. A.; Rowley, R. L. *J. Phys. Chem. A* **1997**, *101*, 5026.

(23) Lahtela, M.; Pakkanen, T. A.; Nissfolk, F. *J. Phys. Chem. A* **1997**, *101*, 5949.

(24) Gupta, S. A.; Cochran, H. D.; Cummings, P. T. *J. Chem. Phys.* **1997**, *107*, 10316.

(25) Gupta, S. A.; Cochran, H. D.; Cummings, P. T. *J. Chem. Phys.* **1997**, *107*, 10327.

(26) Gupta, S. A.; Cochran, H. D.; Cummings, P. T. *J. Chem. Phys.* **1997**, *107*, 10335.

(27) Lee, S. H.; Lee, H.; Pak, H. *Bull. Kor. Chem. Soc.* **1997**, *18*, 501.

(28) Khare, R.; de Pablo, J.; Yethiraj, A. *J. Chem. Phys.* **1997**, *107*, 6956.

(29) Moore, J. D.; Cui, S. T.; Cummings, P. T.; Cochran, H. D. *AIChE J.* **1997**, *43*, 3260

(30) Gupta, S. A.; Cochran, H. D.; Cummings, P. T. *Fluid Phase Equil.* **1998**, *151*, 125.

(31) Lee, S. H.; Cummings, P. T.; *Mol. Simul.* **1998**, *21*, 27.

(32) Lahtela, M.; Linnolahti, M.; Pakkanen, T. A.; Rowley, R. L. *J. Chem. Phys.* **1998**, *108*, 2626.

(33) Cui, S. T.; Cummings, P. T.; Cochran, H. D.; Moore, J. D.; Gupta, S. A. *Int. J. Thermophys.* **1998**, *19*, 449.

(34) Dr. Peter Gordon, Mobil Technology Company, private communication.

(35) Allen, M. P.; Tildesley, D. J. *Computer Simulation of Liquids*; Clarendon: Oxford, 1987.

(36) Evans, D. J.; Morris, G. P. *Statistical Mechanics of Nonequilibrium Liquids*, Academic: London, 1990.

(37) Cummings, P. T.; Evans, D. J. *Ind. Eng. Chem. Res.* **1992**, *31*, 1237.

(38) Martyna G. J.; Tuckerman, M. E.; Tobias, D. J.; Klein, M. L. *Mol. Phys.* **1996**, *87*, 1117.

(39) Martin, M. G.; Siepmann, J. I. *J. Phys. Chem. B* **1998**, *102*, 2569.

(40) Martin, M. G.; Siepmann, J. I. *J. Phys. Chem. B* **1999**, *103*, 4508.

(41) Tuckerman, M.; Berne, B. J.; Martyna, G. J. *J. Chem. Phys.* **1992**, *97*, 1990.

(42) Mundy, C. J.; Siepmann, J. I.; Klein, M. L. *J. Chem. Phys.* **1995**, *103*, 10192.

(43) Hieber, C. A.; Chiang, H. H. *Polym. Eng. Sci.* **1992**, *32*, 931.

(44) Ferry, J. D. *Viscoelastic Properties of Polymers*; John Wiley and Sons: New York, 1970.

(45) Maxwell, J. B. *Data Book on Hydrocarbons*, D. Van Nostrand: New York, 1950.

(46) Runnebaum, R.; Maginn, E. J. *J. Chem. Phys. B* **1997**, *101*, 6394.

(47) Smith, G. D.; Yoon, D. Y. *J. Chem. Phys.* **1994**, *100*, 649.

(48) Rouse, P. E. *J. Chem. Phys.* **1953**, *21*, 1272.

(49) Mondello, M.; Grest, G. S.; Webb, E. B., III; Peczak, P. *J. Chem. Phys.* **1998**, *109*, 798.

(50) Ertl, H.; Dullien, F. A. L. *AIChE J.* **1973**, *19*, 1215.

(51) Chen, B.; Siepmann, J. I. *J. Phys. Chem. B* **1999**, *103*, 5370.

(52) Chynoweth, S.; Coy, R. C.; Michopoulos, Y. *J. Eng. Tribol.* **1995**, *209*, 243.